Journal of
Materials Chemistry C

ROYAL SOCIETY
OF CHEMISTRY

PAPER

View Article Online
View Journal

Cite this: DOI: 10.1039/c9tc05822b

Keto-salicylaldehyde azine: asymmetric substituent effect on their optical properties *via* electron-donating group insertion†

Jialin Tong,‡[a] Kexin Zhang,‡[b] Jing Wang,‡[a] Hui Li,[a] Fan Zhou,[b]
Zhiming Wang,*[abc] Xiaojuan Zhang*[a] and Ben Zhong Tang*[bc]

Organic fluorescent probes have attracted increasing attention owing to their high sensitivity and recognition ability, structurally adjustable flexibility and manifestation in the form of visualization. Salicylaldehyde azine (SAA) and its derivatives exhibit a great potential for practical applications, but the synthesis of SAA asymmetric compounds in low yields, serving multiple functions, is cumbersome. As an alternative building block, Keto-Salicylaldehyde Azine (KSA) was developed by our group for constructing various AIEgens *via* an excited state intramolecular proton transfer (ESIPT) process to detect some cellular organelles and specific metal ions. For illuminating the structure–property relationship of the two asymmetric sides in a KSA unit, DPAS was employed as a model and the *N*,*N*-diethyl group with electron-donating effects was introduced on its salicylaldehyde side (S-terminal) and diphenylketone side (K-terminal). Three new derivatives were obtained and showed different photophysical properties, particularly in AIE performance and metal ion responsiveness, implying that their intrinsic electronic structure can be easily affected by the asymmetric substitution effect. Therefore, this study is a meaningful and valuable reference for KSA modification on expanding fluorescent probes with various functions *via* the purposeful regulation of their chemical structure, by either modifying the K-terminal or the S-terminal.

Received 24th October 2019,
Accepted 26th November 2019

DOI: 10.1039/c9tc05822b

rsc.li/materials-c

1. Introduction

Organic fluorescent probes, as important analytical and detection materials, have attracted increasing attention.[1] Owing to their tunability in chemical structures, they can be designed and constructed into ideal probes according to our various practical needs; and their structures can be constantly optimized in to increase their selectivity and sensitivity.[2] For example, their application in monitoring the nature and concentration of metal ions or anions in various environments is one of the most typical and familiar uses, relevant in our daily lives.[3] However, most organic fluorescent probes with conjugated structures, such as those containing aromatic rings, will inevitably exhibit the aggregation-caused quenching (ACQ) phenomenon in aqueous environments, which is not suitable for their practical applications.[4] The discovery of aggregation-induced emission (AIE) has fundamentally overcome this shortcoming to a large extent,[5] and the development of AIE-based fluorescent probes has gradually become a key research theme.[6]

Salicylaldehyde azine (SAA) is a typical building-block capable of excited-state intramolecular proton transfer (ESIPT),[7] synthesized from hydrazine and salicylaldehyde Schiff-base. SAA derivatives exhibit obvious AIE behaviors with highly distinguishable fluorescence performance and have been widely applied as chemosensors, bioprobes, bioimaging scaffolds, *etc.*[8] These symmetric compounds can be easily synthesized from salicylaldehyde derivatives and hydrazine hydrate at room temperature with high yields (Scheme 1A). Tong *et al.* have given a great contribution to the application of SAA-based derivatives.[9] However, the synthesis of asymmetric SAA derivatives is difficult. Not only an accurate control of the monomers' feed ratio is required, but also the reaction intermediates are easily converted to their symmetric products due to the autocatalytic

---

[a] *School of Petrochemical Engineering, Shenyang University of Technology (SUT), Liaoyang 111003, China. E-mail: 1664392140@qq.com*

[b] *Key Laboratory of Luminescence from Molecular Aggregates of Guangdong Province, State Key Laboratory of Luminescent Materials and Devices, Center for Aggregation-induced emission, South China University of Technology, Guangzhou 510640, China. E-mail: wangzhiming@scut.edu.cn*

[c] *Department of Chemistry, Hong Kong Branch of Chinese National Engineering Research Center for Tissue Restoration and Reconstruction, Department of Chemical and Biological Engineering, The Hong Kong University of Science and Technology, Kowloon, Hong Kong, China. E-mail: tangbenz@ust.hk*

† Electronic supplementary information (ESI) available: The synthesis of compounds, ^{1}H NMR spectra of N-DPAS, 2N-DPAS and 3N-DPAS; Abs spectra of the AIE properties of N-DPAS and 3N-DPAS; I/I_0 emission plots of N-DPAS and 2N-DPAS; The histogram analysis of N-DPAS, 2N-DPAS and 3N-DPAS dots upon addition of the mixture of different ions. See DOI: 10.1039/c9tc05822b

‡ Jialin Tong, Kexin Zhang and Jing Wang contributed equally to this work.

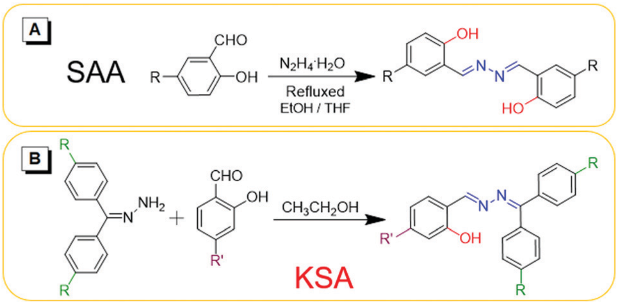

Scheme 1 (A) SAA synthetic route; (B) the synthetic route to obtain KSA.

action (H^+) of salicylaldehyde. In order to break through the bottlenecks of SAA-based derivative syntheses and efficiently prepare more functional asymmetric fluorescence probes, we have constructed and developed a new type of fluorescence probe building-block named keto-salicylaldehyde azine (KSA).[10] Compared to the SAA unit, KSA is easily prepared with fairly high yields from salicylaldehyde derivatives and diaryl-ketone hydrazones, and the latter is either commercial available or easily prepared from the reaction (Scheme 1B) between hydrazine hydrate and diaryl ketone derivatives, without any purification *via* column chromatography. For describing these structures more vividly, we defined the two sides of the azine centre as the K-terminal (from the diaryl ketone end) and the S-terminal (from the salicylaldehyde end). Employing the Friedel–Crafts acylation and the phenolic hydroxyl reaction with urotropine, different diaryl ketone and salicylaldehyde derivatives could be obtained as expected. By changing the peripheral recognition group, these different KSA-based materials showed target imaging and fluorescence switching ability.[10,11]

DPAS was previously reported by our group for lipid droplets-targeting and metal ions probing, and one of its derivatives, named 2M-DPAS, could target lysosomes after introducing two basic morpholine groups linked with six-carbon chains.[10a] Unfortunately, the fundamental electronic effect of this asymmetric KSA structure has not been discussed in detail. In this study, the *N*,*N*-diethyl group was employed as an electron-donating group to introduce on the S-terminal or K-terminal, and three compounds, N-DPAS, 2N-DPAS, and 3N-DPAS, were synthesized; moreover, the effects of intramolecular charge-transfer (CT) and the ESIPT process on their photophysical behaviours were discussed. Fortunately, the asymmetric substitution effect, originating from their intrinsic electronic structure, was observed to affect their functions, particularly the AIE performance and metal ion responsiveness. Hence, we present a meaningful and a valuable review for KSA-modification on expanding fluorescent probes with various functions *via* the purposeful regulation of chemical structures in the K-terminal or the S-terminal.

2. Results and discussion

2.1 Molecule design

As described in Scheme S1 (ESI†), commercial and cheap diaryl ketone and salicylaldehyde derivatives were employed as the raw materials. Under the catalysis of a small amount of a protonic acid (acetic acid), the diaryl ketones reacted with excessive hydrazine hydrate in ethanol to form ketone hydrazone derivatives, which were then cooled to precipitate their crystals, and washed with water to remove excess hydrazine hydrate. The crude products obtained without further purification could directly react with the corresponding salicylaldehyde derivatives to obtain the target structures. Compared to the synthesis route of common fluorescent probes, the preparation cost of these KSA derivatives was lower, which is very meaningful for future practical applications.[12]

Here, the *N*,*N*-diethyl group, a classic electron-donating group, was introduced on KSA's two substitution sides for observing the effects of asymmetry on the luminescence behaviour. In N-DPAS, the *N*,*N*-diethyl group was inserted *para* to the position of the aldehyde group in salicylaldehyde, which could enhance its electron-donating effects owing to resonance with the newly formed azine core in N-DPAS. In order to prevent the effect of cis-trans isomerization on the electronic structure due to the change of the conjugated form of the hydrazine center, two *N*,*N*-diethyl groups were introduced at the K-terminal to form 2N-DPAS. Combining the structural characteristics of the two compounds above, 3N-DPAS was also prepared. Their chemical structures were characterized *via* NMR, high-resolution mass spectroscopy (HRMS), and satisfactory results were obtained. The three derivatives all showed a similar typical intramolecular hydrogen bond formation to DPAS, which highly favors the ESIPT process. Moreover, the diaryl structure at the K-terminal had a certain degree of freedom and rotation ability, which provided a possibility for the restriction of rotation from solution to the aggregate state. All these factors suggest that the three compounds possibly have AIE abilities. In terms of electronic structure distribution, the three derivatives are significantly different from DPAS. In general, the introduction of electron-donating groups leads to the enhancement of the intramolecular CT effect, which usually leads to the quenching of fluorescence in the aggregated state.[13] In addition, as KSA has a typical dentate chelating structure, the change in electron distribution on the phenolic hydroxyl group and the nitrogen atoms in the azine group can also lead to a change in their target recognition ability. In fact, for these positive and negative effects, which one is more beneficial to improve the performance of KSA fluorescent probes is our real concern (Fig. 1).

2.2 Solvation effects

The solvation effect is the most distinctive feature for molecules capable of ESIPT because the nature and polarity of the solvent can directly influence the formation of intramolecular hydrogen bonding.[14] Herein, we chose six solvents to test the absorption (Abs)

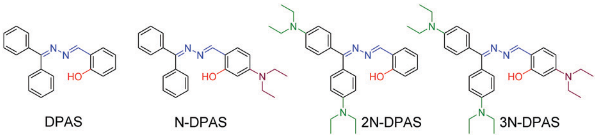

Fig. 1 Chemical structures of DPAS N-DPAS, 2N-DPAS, and 3N-DPAS.

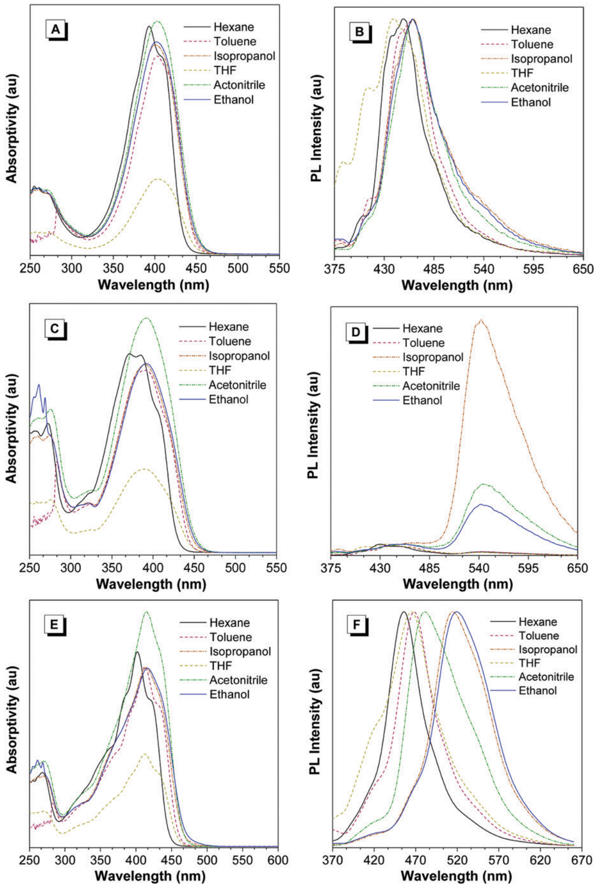

Fig. 2 Abs and PL spectra of N-DPAS (A and B), 2N-DPAS (C and D) and 3N-DPAS (E and F) in different solvents (10^{-5} M).

and photoluminescence (PL) abilities of our compounds, and the results are illustrated in Fig. 2. In a similar way to most of the ESIPT-based compounds,[15] the shifts of their absorption peaks were not significant, suggesting that the polarity of the external environment did not have a significant effect on their ground states. However, these changes became noticeably very complicated in the fluorescence spectra. Unlike their model compound DPAS, with a short-wavelength emission at 425 nm, originating from the E form emission ($E^* \rightarrow E$) and a long-wavelength emission at 550 nm, assigned to the emission of the K form ($K^* \rightarrow K$),[10a] N-DPAS and 3N-DPAS did not show a clear proportional switching trend between E-emissions and K-emissions. However, in 2N-DPAS, the K-emission at 545 nm seemed to have absolute advantage than the E-emission at about 440 nm (Fig. 2D), implying that the energy barrier for the conversion from E* to K* might be relatively small and easily crossed, even in low-polarity solvents, when the *N*,*N*-diethyl groups are only inserted on the K-terminal. For N-DPAS, the E-emission seemed to be dominant, and the red-shift from 440 nm to 460 nm might be due to the intramolecular charge transfer effect caused by the introduction of the electron-donating group at the S-terminal (Fig. 2B). Comparing the two, we speculated that the introduction of electron donors at the K-terminal could enhance the ESIPT process with a benefit on the K-emission, while the intramolecular CT effect might play an important role in the weakening of ESIPT when introducing electron-donating groups at the S-terminal. If both conditions existed at the same time, there would be a competitive relationship. This situation happened precisely in 3N-DPAS, as shown in Fig. 2F, and its PL spectra became visibly very complicated, and shows the sensitivity of the species to the solvent polarity through a red-shift and widening of the peaks, which was very difficult to discuss in detail their every peak source, but it might be very beneficial to selective sensing behaviours in a specific environment with little changes.

2.3 AIE performance

According to our previous reports, the rotations and vibrations of DPAS would be restricted from solution to the aggregate state, leading to the easy formation of intramolecular hydrogen bonds to reduce enol–keto conversion barrier, the RIM and ESIPT process are activated to exhibit AIE performance at K-emission location.[10a] In order to discuss how the aggregation process is affected by the substitution with electron-donating groups and by molecular asymmetry, the absorptivity and PL spectra of N-DPAS, 2N-DPAS and 3N-DPAS were recorded, and are presented in Fig. 3.

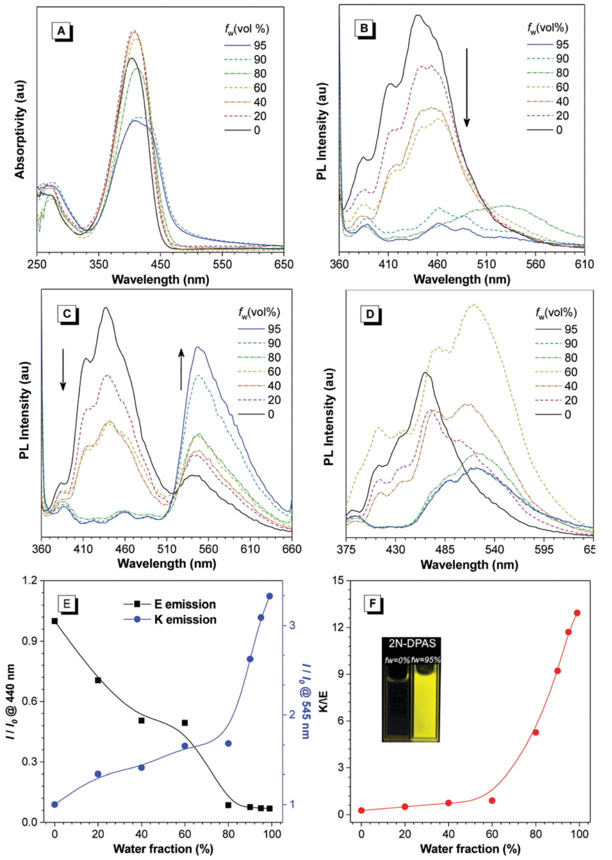

Fig. 3 The Abs spectra of N-DPAS (A) in THF–water mixtures with different water fractions (f_w); The PL spectra of N-DPAS (B), 2N-DPAS (C) and 3N-DPAS (D) in THF–water mixtures with different f_w; E, K (I/I_0 @440 nm and 545 nm) and E/K emission plots of 2N-DPAS (E and F), where I_0 is the PL intensity in pure THF solution.

As shown in Fig. 3A, the absorption band at long wavelength increased in absorption spectra of N-DPAS at $f_w > 60\%$, implying the formation of aggregate structures. Regrettably, this enhanced emission was not significantly visible by naked eye observation under a UV-lamp. As seen in the PL spectra, its E-emission exhibited obvious ACQ in the aggregated state, and its K-emission peak at 530 nm was enhanced very little even for $f_w = 80\%$ (the maximum f_w), which indicates that the ESIPT process is at a disadvantage relative to the dominant CT process. This result was consistent with its solvation behaviour. For 2N-DPAS, as the water content increased, the intensity of the E-emission peak at 440 nm gradually decreased (ACQ), and the intensity of the K-emission peak at 545 nm gradually increased (AIE), implying that the ESIPT process and the restriction of intramolecular rotation (RIR) became protagonists. When $f_w = 90\%$, the spectrum was completely originating from the K-emission, with higher intensity compared to other f_w (Fig. 3C). Based on its photophysical behaviour discussed above, 2N-DPAS showed the phenomenon of enol–keto conversion, which indicates that the introduction of electron-donating groups at the K-terminal makes the E* → K* process easier, and increases the occurrence of ESIPT. Combining ESIPT with the effect of RIM, its significant AIE performance can be explained. Additionally, as shown in Fig. 3E, the signal contrast would be improved by processing mathematically using the classic dual fluorescence-changing process (K-emission/E-emission). 3N-DPAS combined the characteristic of N-DPAS and 2N-DPAS, and its PL spectra were complicated by many factors, such as solvent polarity and aggregation (Fig. 3D). However, in careful comparison, its E-emission located at about 465 nm, and the K-emission was at around 521 nm. Although CT in 3N-DPAS was larger than in 2N-DPAS, the ESIPT process was more active than for N-DPAS. Under the synergistic effect of the RIM process, 3N-DPAS exhibited a weak AIE activity (Fig. S5B, ESI†). In a word, standing at these results, the introduction of electron-donating groups only to the K-terminal of KSAs is very beneficial to constructing AIEgens, which is very important to develop KSA-based fluorescent probes, that can be exploited in their aggregate state.

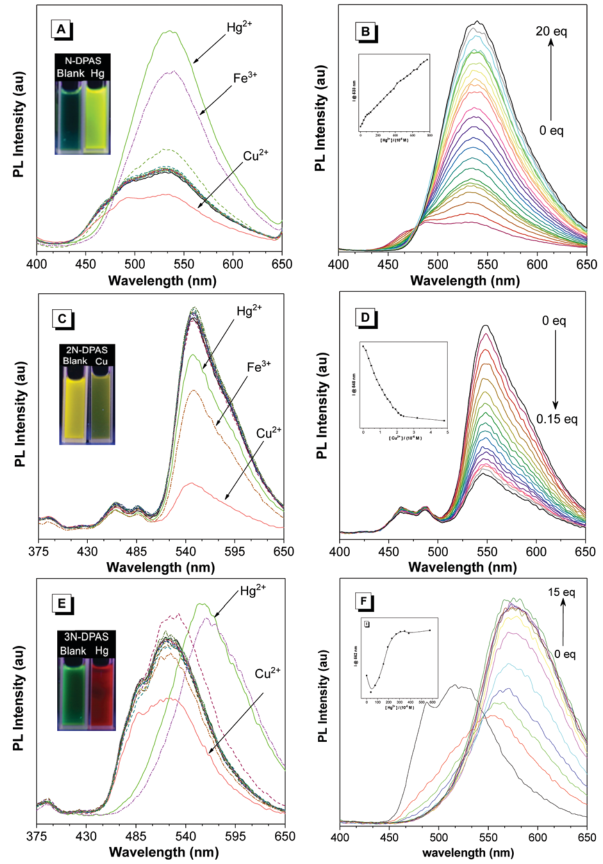

Fig. 4 The changes of PL spectra of N-DPAS (A), 2N-DPAS (C) and 3N-DPAS (E) in the mixture ($f_w^{\text{N-DPAS}} = 80\%$; $f_w^{\text{2N-DPAS}} = 100\%$; $f_w^{\text{3N-DPAS}} = 80\%$) upon addition 5 eq. of respective ions; changes in PL spectra of N-DPAS (B) upon addition of various Hg^{2+} (from 0 to 20 eq.), 2N-DPAS (D) upon addition of various Cu^{2+} (from 0 to 0.15 eq.) and 3N-DPAS (F) upon addition of various Hg^{2+} (from 0 to 15 eq.) in different water fraction (f_w).

2.4 Metal ion selectivity

As typical Schiff base structures, KSA and its derivatives usually have a certain metal ion chelating ability, and they could achieve the selective recognition of metal ions by controlling their molecular and electronic structure, and changing the solvent.[10b] As a model compound, DPAS exhibited good selectivity to Cu^{2+} as a fluorescence quenching ("turn-off" mode) probe with excellent limits of detection (LOD) in aqueous solutions;[10b] but in the three new derivatives, the ion-selective behaviour was expected to change, because the electronic structure of their chelating sites is affected by the different effects of the electron-donating groups. Therefore, 16 metal ions (using their ClO_4^- salts) were employed to explore the probes' selectivities (Fig. 4): Cu^{2+}, Hg^{2+}, Ag^+, Li^+, Na^+, Zn^{2+}, Co^{2+}, Pb^{2+}, Mn^{2+}, Ni^{2+}, Ba^{2+}, Cd^{2+}, Mg^{2+}, Al^{3+}, Ca^{2+}, and Fe^{3+}. Considering their practical application value, the aggregates employed were prepared based on the AIE discussion above, hence they were used with the f_w that achieved the relative higher emission intensity: $f_w^{\text{N-DPAS}} = 80\%$, $f_w^{\text{2N-DPAS}} = 100\%$, and $f_w^{\text{3N-DPAS}} = 80\%$ (defined as blank). By measuring the PL spectra in ion mixtures, the three probes showed some selectivity to Cu^{2+} *via* fluorescence quenching ("turn-off" mode) like DPAS, but there was a significant difference in the degree of chelation at the same ion/probe concentrations, illustrating that these asymmetric substitutions do affect the chelating ability of the probes. As a typical AIE probe, 2N-DPAS showed a quenching effect similar to DPAS, owing to the electron cloud density increment over the N atoms in the azine group when *N*,*N*-diethyl groups are inserted on the K-terminal. After the fluorescence titration process shown in Fig. 4D, the fluorescence intensity of the K-emission at 548 nm gradually decreased with the continuous addition of Cu^{2+}. Based on the curves of the fluorescence quenching ($r^2 = 0.9867$), 2N-DPAS showed a limit of detection of 0.11 μM, which is lower than that of common Cu^{2+} probes with similar structures (like SAA and its derivatives).[8a,9c] Simultaneously, the aggregates of 2N-DPAS exhibited a certain anti-interference ability for Hg^{2+} interference in "turn-on" mode, as shown in Fig. S6B (ESI†), which was better than that of DPAS. The important photophysical data was shown in Table 1.

Table 1 The important photophysical data of three compounds

Compound	λ_{abs} (nm)	λ_{em} (nm)				PLQY (%)		
	Soln[c]	E-emission[a]	K-emission[a]	Add Hg^{2+}[b]	Add Cu^{2+}[b]	Aggregation (f_w = 95%)	Soln (THF)	Solid
N-DPAS	406	441	530	535	—	0.1	0.4	0.9
2N-DPAS	395	440	545	—	548	1.7	0.7	1.3
3N-DPAS	417	465	521	558	—	0.8	0.4	0.7

[a] Max peak locations in the aqueous environment. [b] Max peak locations in the metal ion selectivity. [c] Max peak locations in the THF.

When the *N*,*N*-diethyl group was introduced on the S-terminal, the sensitivity of the probe to Cu^{2+} decreased obviously, while the selectivity to Hg^{2+}/Fe^{3+} increased significantly. In N-DPAS, the fluorescence intensity increased with the addition of Hg^{2+} (as a model), which indicated fluorescent detection in "turn-on" mode. As shown in Fig. 4B, a good linear relationship (r^2 = 0.9931) with a LOD of 6.02 μM was obtained by a titration experiment. Although the LOD for Hg^{2+} was still not ideal, such a simple composite probe, having a fluorescent "turn-on" ability, is still an important tool for rapid detection in practical applications. Certainly, its selectivity needs further improvement in distinguishing Hg^{2+} and Fe^{3+} *via* other means. 3N-DPAS was observed to be less sensitive, in accordance with the discussion on the solvation effect and the AIE performance. 3N-DPAS combined the characteristics of the other two compounds, giving very little response to Cu^{2+} ("turn-off" mode) and Hg^{2+}/Fe^{3+} (enhanced mode), which is not of much practical value. Interestingly, some valuable red-shifts in the PL spectra appeared when Hg^{2+}/Fe^{3+} were added, and the change could be observed by the naked eye from bright green emission to red one under UV-lamp. Employing titration experiments, the LOD for Hg^{2+} was estimated at 7.07 μM (r^2 = 0.9773), similar to that of N-DPAS. However, the fluorescence-induced colour change displays the effects in a more intuitive way. More importantly, the significance of the simultaneous substitution on both terminals was revealed. Comparing the three compounds' performances in ion sensitiveness, S-terminal substitution dominated, which should be due to the electron-donating group being relatively close to the chelating sites leading to more direct electronic effects. At the same time, this observation is very important for us to develop function-oriented KSA probes in the future.

3 Conclusion

As a novel building block for AIEgens construction, KSA has two significant terminals that can be substituted compared to SAA, namely, K-terminal and S-terminal. The discussion of the structure–properties relationship of KSA derivatives becomes very meaningful to expand fluorescent probes application *via* the purposeful regulation of their chemical structure. After inserting the *N*,*N*-diethyl group with an electron-donating effect on the S-terminal of DPAS in the *para*-substituted position of the azine, the CT effect was enhanced with a simultaneous decrement of the ESIPT process, and the AIE performance was not ideal, especially in N-DPAS. However, the two derivatives (N-DPAS and 3N-DPAS) increased the selectivity towards Hg^{2+}/Fe^{3+}, but had a weak response to Cu^{2+}. With its K-terminal substitution, 2N-DPAS gave a good AIE performance with higher selectivity to Cu^{2+} than DPAS, without Hg^{2+}/Fe^{3+} interference. Combining the spectral analysis of the asymmetric substitution effect, the role of the different KSA modifications for various functions became very clear, which is very important when developing function-oriented KSA probes.

Conflicts of interest

The authors declare no competing financial interest.

Acknowledgements

This work was financially supported by the National Natural Science Foundation of China (21788102, 51673118 and 21975077), the Science & Technology Program of Guangzhou (201804010218 and 201804020027), the Innovation and Technology Commission of Hong Kong (ITC-CNERC14SC01), the Fundamental Research Funds for the Central Universities (2019ZD04) and the Fund of Key Laboratory of Luminescence from Molecular Aggregates of Guangdong Province (2019B030301003).

Notes and references

1 (*a*) J. Zhang, Y. Zhou, J. Yoon and J. Kim, *Chem. Soc. Rev.*, 2011, **40**, 3416–3429; (*b*) J. Kolanowski, F. Liu and E. New, *Chem. Soc. Rev.*, 2018, **47**, 195–208; (*c*) W. Lu, X. Qin, S. Liu, G. Chang, Y. Zhang, Y. Luo, A. Asiri, A. Al-Youbi and X. Sun, *Anal. Chem.*, 2012, **84**, 5351–5357; (*d*) A. Ogasawara, M. Kamiya, K. Sakamoto, Y. Kuriki, K. Fujita, T. Komatsu, T. Ueno, K. Hanaoka, H. Onoyama, H. Abe, Y. Tsuji, M. Fujishiro, K. Koike, M. Fukayama, Y. Seto and Y. Urano, *Bioconjugate Chem.*, 2019, **30**, 1055–1060.

2 (*a*) Y. Urano, M. Kamiya, K. Kanda, T. Ueno, K. Hirose and T. Nagano, *J. Am. Chem. Soc.*, 2005, **127**, 4888–4894; (*b*) Z. Xiang, Z. Wang, T. Ren, W. Xu, Y. Liu, X. Zhang, P. Wu, L. Yuan and X. Zhang, *Chem. Commun.*, 2019, **55**, 11462–11465; (*c*) M. Sakabe, D. Asanuma, M. Kamiya, R. Iwatate, K. Hanaoka, T. Terai, T. Nagano and Y. Urano, *J. Am. Chem. Soc.*, 2013, **135**, 4926–4929.

3 (*a*) Y. Dong, R. Wang, G. Li, C. Chen, Y. Chi and G. Chen, *Anal. Chem.*, 2012, **84**, 6220–6224; (*b*) D. Huang, C. Niu, M. Ruan, X. Wang, G. Zeng and C. Deng, *Environ. Sci. Technol.*, 2013, **47**, 4392–4398; (*c*) A. Klymchenko, *Acc. Chem. Res.*, 2017, **50**, 366–375; (*d*) A. Said, N. Georgiev and V. Bojnov, *Spectrochim. Acta, Part A*, 2019, **223**, 117304; (*e*) M. Wang, C. Cheng, C. Li, D. Wu, J. Song, J. Wang,

X. Zhou, H. Xiang and J. Liu, *J. Mater. Chem. C*, 2019, **7**, 6767; (*f*) X. Zhang, J. Shi, G. Shen, F. Guo, J. Cheng, X. Zhou and H. Xiang, *Mater. Chem. Front.*, 2017, **1**, 1041.

4 D. Ding, K. Li, B. Liu and B. Z. Tang, *Acc. Chem. Res.*, 2013, **46**, 2441–2453.

5 (*a*) T. Förster and K. Kasper, *Z. Phys. Chem.*, 1954, **1**, 275–277; (*b*) Y. Hong, J. Lam and B. Z. Tang, *Chem. Soc. Rev.*, 2011, **40**, 5361–5388; (*c*) J. Mei, Y. Hong, J. Lam, A. Qin, Y. Tang and B. Z. Tang, *Adv. Mater.*, 2014, **26**, 5429–5479; (*d*) J. Mei, N. Leung, R. Kwok, J. Lam and B. Z. Tang, *Chem. Rev.*, 2015, **115**, 11718–11940.

6 (*a*) H. Tong, Y. Hong, Y. Dong, M. Häussler, Z. Li, J. Lam, Y. Dong, H. Sung, L. Williams and B. Z. Tang, *J. Phys. Chem. B*, 2007, **111**, 11817–11823; (*b*) M. Gao, C. Sim, C. Leung, Q. Hu, G. Feng, F. Xu, B. Z. Tang and B. Liu, *Chem. Commun.*, 2014, **50**, 8312–8315; (*c*) Y. Li, R. Xie, X. Pang, Z. Zhou, H. Xu, B. Gu, C. Wu, H. Li and Y. Zhang, *Talanta*, 2019, **205**, 120143; (*d*) S. Gan, J. Zhou, T. Smith, H. Su, W. Luo, Y. Hong, Z. Zhao and B. Z. Tang, *Mater. Chem. Front.*, 2017, **1**, 2554–2558.

7 (*a*) Y. Shen, M. Li, M. Yang, Y. Zhang, H. Li and X. Zhang, *Spectrochim. Acta, Part A*, 2019, **222**, 117230; (*b*) L. Peng, L. Xiao, Y. Ding, Y. Xiang and A. Tong, *J. Mater. Chem. B*, 2018, **6**, 3922–3926.

8 (*a*) Z. Wang, F. Zhou, J. Wang, Z. Zhao, A. Qin, Z. Yu and B. Z. Tang, *Sci. China: Chem.*, 2018, **61**, 76–87; (*b*) M. Ziółek, J. Kubicki, A. Maciejewski, R. Naskręcki and A. Grabowska, *Phys. Chem. Chem. Phys.*, 2004, **6**, 4682–4689; (*c*) Y. Zhao, Y. Li, Y. Long, Z. Zhou, Z. Tang, K. Deng and S. Zhang, *Tetrahedron Lett.*, 2017, **58**, 1351–1355.

9 (*a*) W. Tang, Y. Xiang and A. Tong, *J. Org. Chem.*, 2009, **74**, 2163–2166; (*b*) X. Chen, R. Wei, Y. Xiang, Z. Zhou, K. Li, P. Song and A. Tong, *J. Phys. Chem. C*, 2011, **115**, 14353–14359; (*c*) X. Chen, Y. Xiang, Z. Li and A. Tong, *Anal. Chim. Acta*, 2008, **625**, 41–46.

10 (*a*) Z. Wang, C. Gui, E. Zhao, J. Wang, X. Li, A. Qin, Z. Zhao, Z. Yu and B. Z. Tang, *ACS Appl. Mater. Interfaces*, 2016, **8**, 10193–10200; (*b*) Z. Wang, F. Zhou, C. Gui, J. Wang, Z. Zhao, A. Qin and B. Z. Tang, *J. Mater. Chem. C*, 2018, **6**, 11261–11265.

11 (*a*) R. Hu, F. Zhou, T. Zhou, J. Shen, Z. Wang, Z. Zhao, A. Qin and B. Z. Tang, *Biomaterials*, 2018, **187**, 47–54; (*b*) W. Zhang, F. Zhou, Z. Wang, Z. Zhao, A. Qin and B. Z. Tang, *Chem. – Asian J.*, 2019, **14**, 1662–1666.

12 (*a*) P. Zhang, X. Nie, M. Gao, F. Zheng, A. Qin, S. Wu and B. Z. Tang, *Mater. Chem. Front.*, 2017, **1**, 838–845; (*b*) Z. Peng, Y. Ji, Z. Huang, B. Tong, J. Shi and Y. Dong, *Mater. Chem. Front.*, 2018, **2**, 1175–1183; (*c*) H. Yu, J. Zhi, Z. Chang, T. Shen, W. Ding, X. Zhang and J. Wang, *Mater. Chem. Front.*, 2019, **3**, 151–160.

13 P. Zhang, X. Guo, Y. Xiao, Q. Zhang and C. Ding, *Spectrochim. Acta, Part A*, 2019, **223**, 117318.

14 (*a*) M. Li, W. Ren, Z. He and Y. Zhu, *J. Cluster Sci.*, 2017, **28**, 2111–2122; (*b*) Y. Qi, M. Lu, Y. Wang, Z. Tang, Z. Gao, J. Tian, X. Fei, Y. Li and J. Liu, *Org. Chem. Front.*, 2019, **6**, 3136–3143.

15 (*a*) S. Dennison, J. Guharay and P. Sengupta, *Spectrochim. Acta, Part A*, 1999, **55**, 1127–1132; (*b*) S. Chen, P. Hou, J. Wang and X. Song, *RSC Adv.*, 2012, **2**, 10869–10873; (*c*) M. Gao, Q. Hu, G. Feng, B. Z. Tang and B. Liu, *J. Mater. Chem. B*, 2014, **2**, 3405–3558.